



## ICESat over Arctic sea ice: Estimation of snow depth and ice thickness

R. Kwok<sup>1</sup> and G. F. Cunningham<sup>1</sup>

Received 28 January 2008; revised 19 May 2008; accepted 29 May 2008; published 7 August 2008.

[1] Starting with retrieved freeboards from four ICESat campaigns (ON05, October/November 2005; FM06, February/March 2006; ON06, October/November 2006; and MA07, March/April 2007) we estimate their ice thicknesses using constructed fields of daily snow depth and compare them with ice drafts from moored upward-looking sonars. The methodologies, considerations, and assumptions used in the conversion of freeboard to ice thickness are discussed. The thickness distributions of the Arctic multiyear and seasonal ice covers are contrasted. Broadly, the resulting fields seem seasonally and interannually consistent in terms of thickness, growth and ice production. We find mean thicknesses of 2.15/2.46 m in ON05/FM06 and an overall thinner ice cover of 1.96/2.37 m in ON06/MA07. This represents a growth of  $\sim 0.3$  m and  $\sim 0.4$  m during the  $\sim 4$ -month intervals of the ON05-FM06 and ON06-MA07 campaigns, respectively. After accounting for data gaps, we compute overall Arctic Ocean ice volumes of 11,318, 14,075, 10,626, and 13,891 km<sup>3</sup> for the ON05, FM06, ON06, and MA07 campaigns, respectively. The higher total volume in ON05 (versus ON06) can be attributed to the higher multiyear ice coverage that fall: 37% versus 31%. However, the higher estimated ice production (less export) during the second year (3265 versus 2757 km<sup>3</sup>) is likely due to the higher growth rate over the larger expanse of seasonal sea ice during the fall and winter. Inside a 25-km radius of two mooring locations in the Beaufort Sea, the estimated mean ICESat ice drafts from ON05 and FM06 are within 0.5 m of those measured at the moorings.

**Citation:** Kwok, R., and G. F. Cunningham (2008), ICESat over Arctic sea ice: Estimation of snow depth and ice thickness, *J. Geophys. Res.*, 113, C08010, doi:10.1029/2008JC004753.

### 1. Introduction

[2] There is a compelling need for a basin-scale picture of Arctic sea ice thickness. Recent submarine-based measurements indicate that the thickness of sea ice in some parts of the central Arctic has decreased at a remarkably high rate over the past few decades [Rothrock *et al.*, 1999; Wadhams and Davis, 2000]. On the basis of analysis of ice draft from overlapping submarine tracks, Rothrock *et al.* [1999] report that the sea ice thinned by  $\sim 1.3$  m in the 1990s relative to the period 1958–1976. Several recent studies, however, argue that changes in the atmospheric circulation are chiefly responsible for the thickness change measured by the submarines [Tucker *et al.*, 2001; Holloway and Sou, 2002; Rothrock *et al.*, 2003]. In particular, Holloway and Sou [2002] suggest that the thickness change averaged over the limited area measured by submarines is higher than the basin average owing to a redistribution of ice volume by surface winds. Their model results attribute this to the convergence of sea ice just west of the Canadian Arctic Archipelago, outside of the submarine data boundary.

[3] Spaceborne remote sensing addresses this need for basin-scale coverage. Current sensors, however, can see only radiation emitted or scattered from the top surface or

the volume within the top few tens of centimeters of the ice and do not see the lower surface. Combining accurate altimetric freeboard with the assumption of hydrostatic equilibrium has been one approach to determine ice thickness. In fact, this forms the algorithmic basis for derivation of sea ice thickness from ESA's planned CryoSat-2 radar altimeter [Wingham *et al.*, 2006]. The tenfold multiplication of freeboard uncertainties in the estimation of ice thickness is daunting and places stringent demands on measurement accuracy. For NASA, recent efforts have been focused on the determination of ice thickness from ICESat elevation profiles. ICESat, launched in January of 2003, carries the Geoscience Laser Altimeter System (GLAS) with one of two channels of the instrument (at 1064 nm) used for surface altimetry [Zwally *et al.*, 2002]. With a beam width of  $\sim 110$   $\mu$ rad and a pulse rate of 40 per second, it profiles the Earth's surface from an orbit with inclination of  $94^\circ$  with footprints of  $\sim 70$  m in diameter spaced at  $\sim 170$ -m intervals. The Arctic Ocean is covered to  $86^\circ$ N. Expected accuracy in elevation determination over relatively low-slope surfaces (e.g., ice sheet) is  $\sim 14$  cm. With a measurement precision of several centimeters, it is a potentially useful instrument for the determination of sea ice freeboard and thickness. An added complication for ice thickness estimation from laser ranging is that echoes originate from the air/snow interface: the hydrostatic loading of the snow layer has to be accounted for. For ICESat, several approaches for freeboard retrieval have been published [Kwok *et al.*, 2004a;

<sup>1</sup>Jet Propulsion Laboratory, California Institute of Technology, Pasadena, California, USA.

*Forsberg and Skourup*, 2005; *Kwok et al.*, 2006, 2007]. *Zwally et al.* [2008] have provided an examination of using ICESat data for obtaining thickness estimates of sea ice in the Weddell Sea. Many investigators are working toward accurate freeboard and thickness retrievals for addressing current gaps and providing future estimates of these parameters.

[4] The subject of this paper pertains to the estimation of ice thickness from ICESat elevations. The starting point of this work is the fields of ICESat freeboard discussed in a recent paper [*Kwok et al.*, 2007]. In that paper, they discuss the identification of suitable sea surface references (tiepoints), a crucial first step for computation of freeboard. Three approaches that provide sea surface tiepoints of different qualities are described. The best quality tiepoints are from those of young ice in new openings identified in near-coincident ICESat profiles and SAR imagery. Tiepoints of an intermediate quality are obtained by examining the reflectivity of samples that are below the background ice together with the expected deviation of their elevations from a mean surface. A third category is identified by using only the expected deviation of their elevations from a mean surface. The strength of the second and third approaches is that they do not depend on SAR imagery and they offer a larger number of tiepoints for providing a more complete view of the spatial pattern of sea ice freeboard over the Arctic Basin. Their results suggest that these retrieval procedures could provide consistent freeboard estimates along 25-km ICESat segments with uncertainties of better than 7 cm. In this paper, we undertake the next steps to convert total freeboard (snow and ice) to ice thickness. The focus is on the various issues associated with the spatial and temporal distribution of snow depth, and the physical properties of snow and ice that are required in the computation of ice thickness. We should note, at the outset, that there are many unknowns in the conversion process and we will alert the reader where assumptions are made to fill those gaps in our knowledge.

[5] The paper is organized as follows. Section 2 describes the ICESat products and ancillary data sets used in our analyses. The relationships between ICESat elevation, freeboard, sea surface height and tiepoints are described in section 3. A nominal adjustment to the freeboard estimates based on the dependence of sea ice reflectivity on snow depth has been added. The next section outlines the construction of the daily fields of snow depth over sea ice. It includes a discussion of seasonal variability in snow density for computation of snow loading. Section 5 provides the details in the estimation of ice thickness using the daily fields of snow depth and total freeboard. The consistencies of the thickness composites are examined in terms of their spatial variability and changes during the approximately four months between acquisitions. In section 6, ice drafts from two moorings in the Beaufort Sea are used to assess the derived ICESat thicknesses. The next to the last section estimates the overall Arctic Ocean ice volume during the four ICESat campaigns. The last section concludes the paper.

## 2. Data Description

### 2.1. ICESat Data

[6] The four ICESat sea ice data sets used in this paper are acquired by Lasers 3d, 3e, 3g and 3h. These laser

campaigns span a period of 35 days during the fall of 2005 (21 October through 24 November), 34 days during the winter of 2006 (22 February through 27 March), 33 days during the fall of 2006 (25 October through 27 November), and 33 days during the winter of 2007 (12 March through 14 April). The ICESat data products are of Release 428, the latest and best releases available in terms of precision orbit and attitude determination at the time of this writing. Henceforth, these four laser operational periods will be referred to as ON05, FM06, ON06, and MA07. In this paper, we focus on the use of freeboards from the first two ICESat campaigns (ON05 and FM06) to illustrate the freeboard/thickness conversion process and to assess the seasonal consistency of the estimates. The additional two thickness fields (ON06 and MA07) are introduced in section 7 for examination of the interannual and seasonal consistencies of thickness and growth among the four fields.

### 2.2. Other Data Sets

[7] Gridded fields of multiyear (MY) ice fraction are from the analysis of QuikSCAT data [*Kwok*, 2004]. QuikSCAT is a moderate resolution wide-swath (1800 km)  $K_u$ -band scatterometer that provides daily coverage of the Arctic Ocean at V- and H-polarizations at incidence angles of  $53^\circ$  and  $45^\circ$ . Daily ice motion fields here are derived from AMSR-E satellite passive microwave observations (89 GHz channel) using the procedures from *Kwok et al.* [1998]. Daily ice concentration fields are also from AMSR-E. The ECMWF meteorological fields are provided by the Data Support Section of the Scientific Computing Division at the National Center for Atmospheric Research (NCAR). These fields are on a Gaussian (n80) grid with a resolution of approximately  $1.125^\circ$ .

## 3. ICESat Freeboard

[8] In this section, we describe: (1) the three categories of sea surface tiepoints used in the retrieval of freeboard; (2) a snow depth adjustment to these estimated sea surface elevations; and (3) a brief summary of the ON05 and FM06 freeboards used in this paper.

### 3.1. Terminology

[9] ICESat freeboard, as used here, is defined as the vertical distance between the air-snow interface and the local sea surface. For the Arctic Ocean, the total freeboard consists generally of a snow layer superimposed on the freeboard of floating sea ice. This total freeboard height,  $h_f$ , above the sea surface can be written as the sum of two terms (Figure 1),

$$h_f = h_{fs} + h_{fi}, \quad (1)$$

where  $h_{fs}$  and  $h_{fi}$  are the thicknesses of the snow and ice layers above the sea surface. Throughout this paper, freeboard generally refers to the total freeboard,  $h_f$ , unless noted otherwise.

[10] The total freeboard,  $h_f$ , is the difference between surface elevation,  $h_s$ , as measured by an altimeter and the sea surface height,  $h_{ssh}$ ,

$$h_f(x, t_i) = h_s(x, t_i) - h_{ssh}(x, t_i). \quad (2)$$

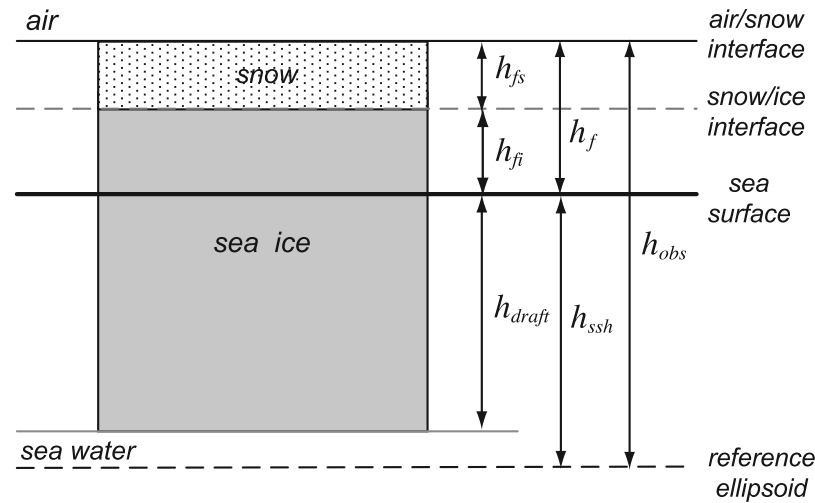


**Figure 1.** Schematic showing the variables of freeboard, draft, and thickness discussed in section 3.

Both  $h_s$  and  $h_{ssh}$  are defined, in the case of ICESat, relative to the TOPEX/POSEIDON ellipsoid.

[11] As mentioned above, the starting point of this paper is the ICESat freeboard from the retrieval procedures described by *Kwok et al.* [2007]; we direct the reader to this paper for more details on freeboard retrieval. Briefly, the freeboard is derived by combining the sea surface estimates ( $h_{ssh}$ ) from three different procedures for identifying ICESat samples suitable for use as  $h_{ssh}$  tiepoints. In

order of quality, these approaches use elevation samples: (1) of new openings identified in ICESat profiles and SAR imagery; (2) where the ICESat reflectivities are below that of the background snow covered sea ice and where their elevations exceed an expected deviation below that of a local mean surface; and, (3) where the only condition is that their elevations exceed an expected deviation below that of a local mean surface. We designate these three categories of tiepoints as  $H_{op}$ ,  $H_{\Delta R}$ , and  $H_{\sigma}$ . The strength of the second

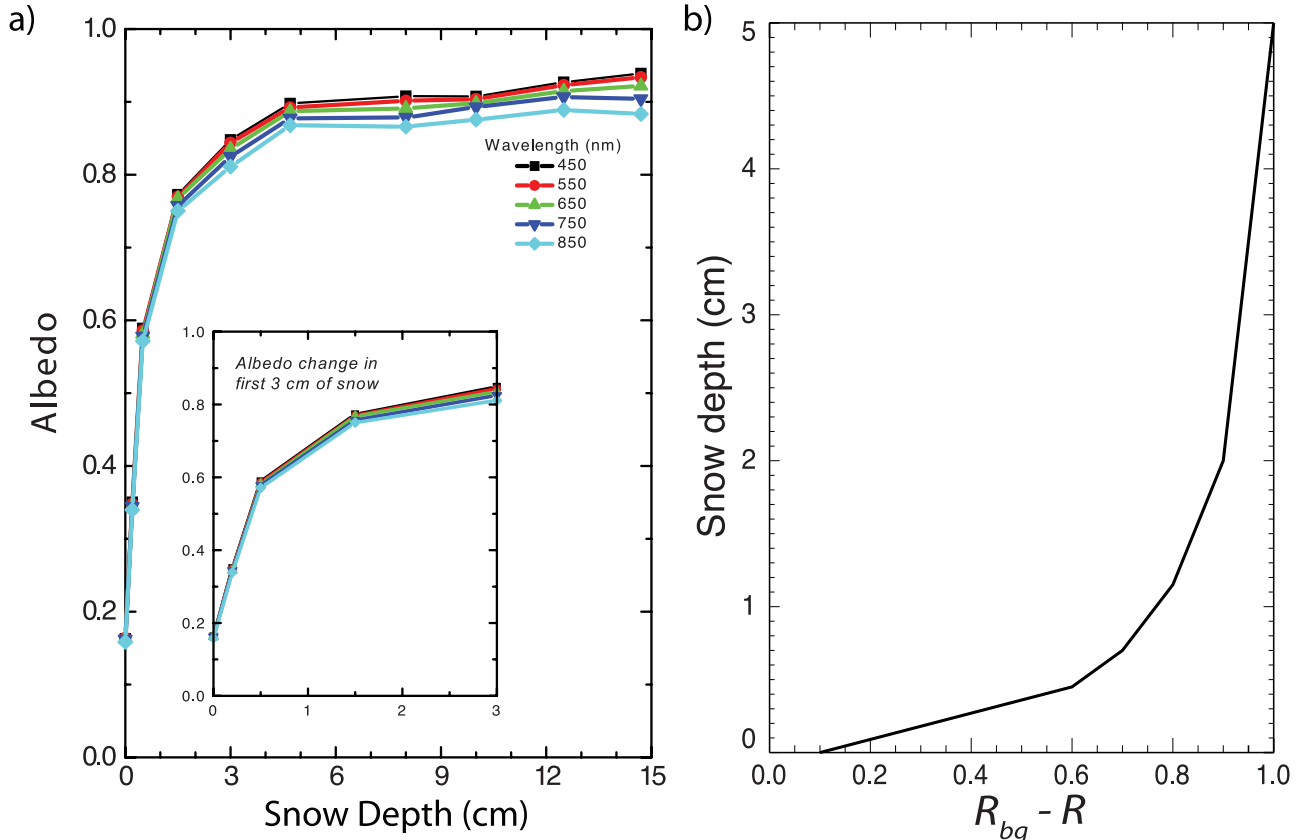


**Figure 2.** (a) Effect of snow depth on the albedo of sea ice (provided by D. Perovich). (b) Nominal adjustment of elevation using difference in reflectivity of the surrounding ice and that of the ICESat sample.

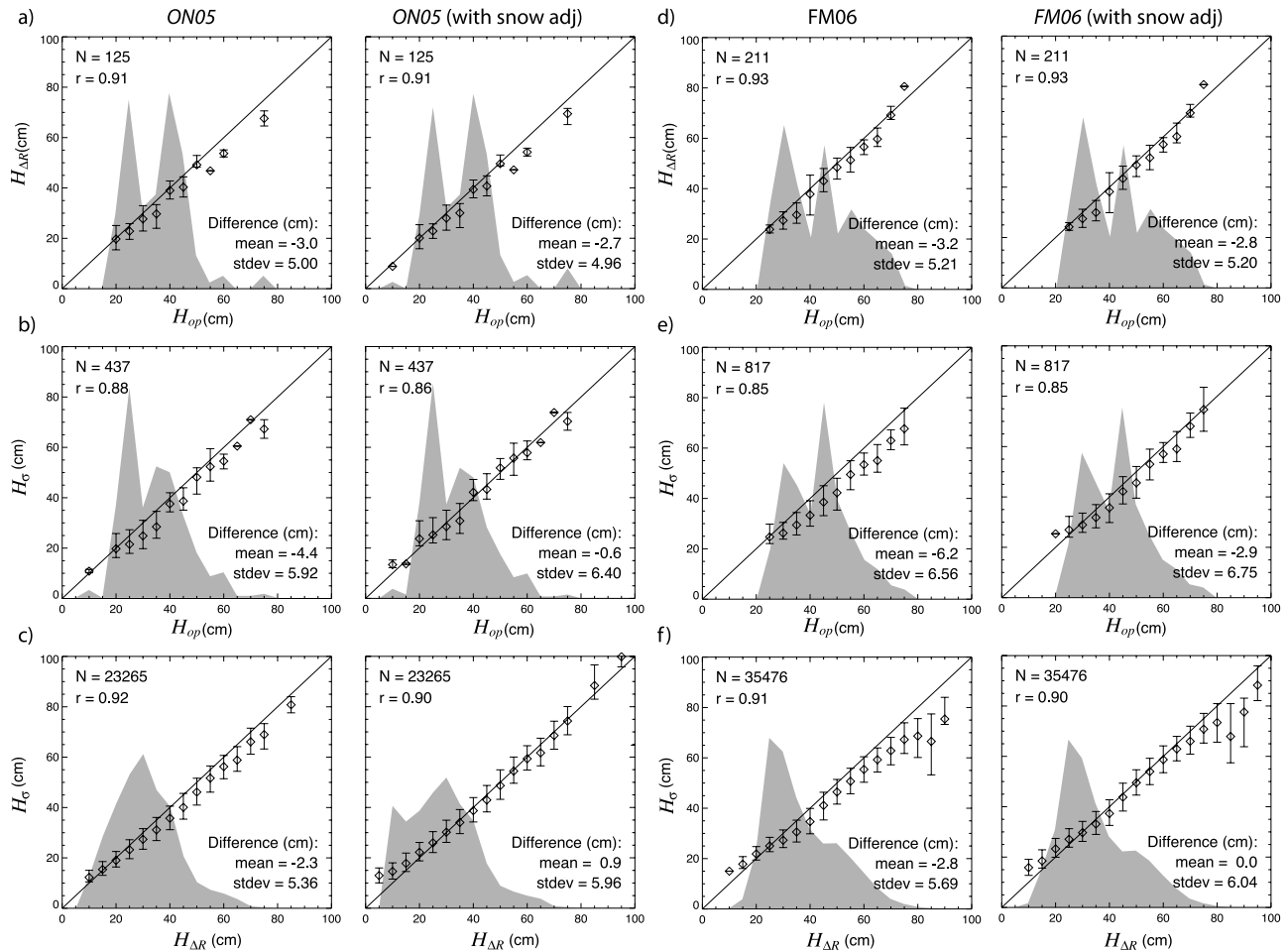


**Figure 3.** Comparisons of the three categories of retrieved freeboard ( $H_{op}$ ,  $H_{\Delta R}$ , and  $H_{\sigma}$ ) before and after the nominal adjustments of snow depth for two campaigns: ON05 and FM06. (a)  $H_{\Delta R}$  versus  $H_{op}$  in ON05. (b)  $H_{\sigma}$  versus  $H_{op}$  in ON05. (c)  $H_{\sigma}$  versus  $H_{\Delta R}$  in ON05. (d)  $H_{\Delta R}$  versus  $H_{op}$  in FM06. (e)  $H_{\sigma}$  versus  $H_{op}$  in FM06. (f)  $H_{\sigma}$  versus  $H_{\Delta R}$  in FM06. Circles/bars represent the means/standard deviations of the samples within 5-cm bins. Histograms (in gray) show the relative distributions of the sample populations on the  $x$  axis.

and third approaches is that they do not depend on the availability of SAR imagery and offer a larger number of tiepoints for providing a more complete view of the spatial pattern of sea ice freeboard over the Arctic Basin. Using the tiepoints from new openings ( $H_{op}$ ) for assessment of the second and third categories ( $H_{\Delta R}$  and  $H_{\sigma}$ ), Kwok *et al.* [2007] showed that the consistency in the identification of individual tiepoints from these two approaches is  $\sim 5$  cm. Overall, their results suggest that the retrieval procedures could provide consistent freeboard estimates along 25-km segments (containing  $\sim 140$  ICESat samples) with uncertainties of better than 7 cm (with a fraction of that due to a bias of  $\sim 3$ –4 cm). The source of these biases is discussed next.

### 3.2. Snow Depth Adjustment

[12] The above procedures for obtaining  $H_{\Delta R}$  and  $H_{\sigma}$  are expected to underestimate the freeboard for two reasons. First, the ICESat elevations represent the mean surface elevations within the illuminated laser spot and our approaches (described by Kwok *et al.* [2007]) to locate the elevation of the lowest surfaces within a given spot (i.e., local sea surface) would be contaminated by the surface

relief of the neighboring ice cover within the footprint. This mixture of surface elevations would contaminate the desired tiepoint elevation and result in an underestimation of the retrieved freeboard. Second, if there were a snow layer over very thin ice, the thickness of the snow would increase the elevation of the sea surface tiepoints and contribute to an underestimation of freeboard.

[13] At this point, we do not have a correction for the possible biases due to a mixture of surface elevations within a laser spot. Here, we address the biases from snow covered ICESat samples with a nominal adjustment of the tiepoint elevations that was not considered by Kwok *et al.* [2007]. This adjustment is based on the steep increase in the reflectivity of sea ice surfaces with the initial deposition of a thin snow layer (Figure 2a). Since we expect the ice in new openings to exhibit low reflectivity, the elevations of the third category of tiepoints ( $H_{\sigma}$ ), and less so the second ( $H_{\Delta R}$ ), are biased because there are no strict requirements on reflectivity. To first order, we can adjust the tiepoint elevations on the basis of their observed reflectivity: we refer to this as a nominal adjustment because the dependence of sea ice reflectivity on snow depth becomes

insignificant beyond 5 cm (see Figure 2b). The elevations of the tiepoints ( $H$ ) are adjusted as follows:

$$H' = H + f(R_{bg} - R). \quad (3)$$

$R_{bg} - R$  is the difference in reflectivity between the newly formed snow covered ice and that of the neighboring ICESat samples, and  $f(R_{bg} - R)$  is the adjustment function shown in Figure 2b. We apply this to all the selected ICESat tiepoints.

[14] To assess the effectiveness of these adjustments, we cross-compare the three estimates of  $H_{op}$ ,  $H_{\Delta R}$ , and  $H_{\sigma}$  before and after the application of the above adjustment. Since the  $H_{op}$  estimates from near coincident ICESat/SAR data are clearly our best available estimates (they are less than a day or two old sea ice surfaces with low reflectivities), we can assess the quality of  $H_{\Delta R}$  and  $H_{\sigma}$  with that of  $H_{op}$ . We can also compare  $H_{\Delta R}$  and  $H_{\sigma}$  with each other because the  $H_{\Delta R}$ 's are of higher quality. The differences are computed for estimates that are within 12.5 km of each other. So that these assessments are between unique tiepoints, duplicated estimates are removed from the three lists.

[15] Figure 3 shows the computed differences and scatter between the three categories of tiepoints for the two ICESat campaigns in ON05 and FM06. The three rows of Figure 3 show the comparisons:  $H_{\Delta R}$  versus  $H_{op}$ ;  $H_{\sigma}$  versus  $H_{op}$ ; and  $H_{\sigma}$  versus  $H_{\Delta R}$ , before and after the snow depth adjustments. We do not expect significant improvements in the comparison between  $H_{\Delta R}$  and  $H_{op}$  (Figures 3a and 3d) after the adjustments because the  $H_{\Delta R}$  retrieval procedures already require the reflectivity of the selected tiepoints to be at least 0.3 below that of the background. However, notable reductions in the mean differences can be seen in the  $H_{\sigma}$  versus  $H_{op}$  and  $H_{\sigma}$  versus  $H_{\Delta R}$  comparisons after the adjustments. In the  $H_{\sigma}$  versus  $H_{op}$  comparisons (Figures 3b and 3e), the mean differences are reduced from  $-4.4$  to  $-0.6$  cm in ON05, and from  $-6.2$  to  $-2.9$  cm in FM06. Similarly, for the  $H_{\sigma}$  versus  $H_{\Delta R}$  comparisons (Figures 3c and 3f), the mean differences are reduced from  $-2.3$  to  $0.9$  cm in ON05, and from  $-2.8$  to  $-0.0$  cm in FM06. The standard deviations are not expected to change significantly in all the cases because the adjustments represent an attempt to improve the estimation of the mean level of the tiepoint surfaces. Overall, the above assessment demonstrates that, for both seasons, this nominal adjustment seems to be effective in removing some of the relative biases in sea surface elevations due to snow coverage.

### 3.3. ON05 and FM06 Freeboards

[16] The three categories of tiepoints are used to provide the best estimate of the sea surface elevation within each 25-km segment along an ICESat track; the scheme is described by Kwok *et al.* [2007]. Figure 4 shows the maps of retrieved freeboards from the ON05 and FM06 campaigns on a 25-km grid. These freeboard estimates include the snow depth adjustments described above. The value at each grid element represents the mean freeboard (Figure 4b) of all 25-km ICESat segments that fall within the grid cell. Only 25-km ICESat segments that contain sea surface estimates are used in the construction of these maps. The number of segments that go into a grid element varies on the basis of ICESat orbits. At high latitudes, the densities are

higher because of convergence of the ground tracks. The overall freeboard distribution is shown in Figure 4c. The ice cover has a mean freeboard of 37.6 cm in ON05. The overall freeboard of 44.6 cm 4 months later (in FM06) represents an increase of 7 cm; this includes ice growth and snow accumulation.

[17] One complicating factor in assessing the seasonal changes in freeboard differences is the varying spatial coverage of multiyear ice due to advection. Even as a broad measure of the seasonal changes, a simple spatial difference between the freeboard fields would mix first-year (FY) and multiyear (MY) samples and give unrealistically large differences when the effects of ice motion are not considered. Instead, in our assessment of these fields, we separate the FY and MY samples with spatial masks of the two primary ice types derived from the analyzed QuikSCAT maps of MY fraction in Figure 4a. To examine only the freeboard changes over the predominantly MY ice cover, all grid cells with less than 0.75 MY fraction are masked out (Figure 4d). Conversely, for examination of the primarily FY ice cover only grid cells with MY fractions of less than 0.25 are included (Figure 4e). The choice of 0.75 and 0.25 MY fraction isopleths for delineating the nearly pure ice zones is quite arbitrary, but the extremes serve to contrast the seasonal changes in MY and FY freeboards. As indicated in Figure 4a, the two zones contain more than 70% of the total ice area.

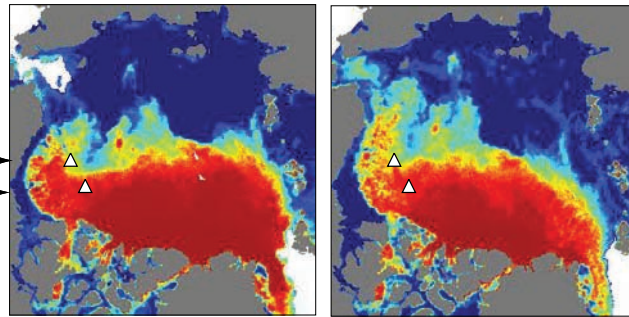
[18] The increase in the mean freeboard of the MY sea ice cover between ON05 and FM06 is 11.5 cm, starting with a mean of 43.0 cm in ON05. In ON05, the mean freeboard of the seasonal ice cover is only 18.6 cm with an increase in freeboard of 11.3 cm. The MY and FY ice cover have comparable increases in mean freeboard; these differences are larger than the overall difference of 7 cm because of the changes in the MY and FY coverage during the fall and winter. In addition, the freeboard distributions of the seasonal ice cover are sharply peaked (with standard deviations of  $\sim 9$ – $15$  cm) in both the fall and winter; this can be attributed to the fact that the seasonal ice cover is formed quite quickly at end of summer and therefore the samples have similar age. The higher variability in the age and deformation of the MY ice cover contribute to its larger SD (of 21–25 cm). The snow, effective snow, and ice thickness panels of Figure 4 will be discussed in sections 4.5, 5.2, and 5.3, respectively.

[19] In contrast to the low-resolution gridded fields, the finer-scale freeboard differences in distributions are shown in Figure 5. Figure 5 is similar to Figures 11 and 12 of Kwok *et al.* [2007] except that the results now include the snow adjustments. Each distribution is constructed using the freeboard estimates of individual ICESat samples ( $\sim 70$  m spots) from 25-km segments that contain sea surface references. Each square in Figure 5 is 700 km on a side. For each region, we show the distributions in ON05 and FM06 and computed statistics (mean and standard deviation). The sharply peaked distributions of the seasonal ice cover during both the fall and winter stand out. Freeboard extremes in the ON05 range from the region over the East Siberian Shelf (14.1 cm) to north of the Greenland Coast (54.3 cm). Similarly, the lowest freeboard in FM06 can be found just east of the New Siberian Islands (26.7 cm) while the highest freeboard remains just north of Greenland (59.7 cm). The longer tails and higher SD in the distributions with higher

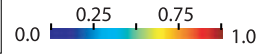
a) MY fraction (MYf)

Nov 15, 2005  
 Coverage:  
 MYf > 0.75 : 37%  
 MYf < 0.25 : 44%

Mooring A →  
 Mooring C →



March 1, 2006  
 Coverage:  
 MYf > 0.75 : 29%  
 MYf < 0.25 : 45%



b) Freeboard Snow Effective Snow Ice Thickness

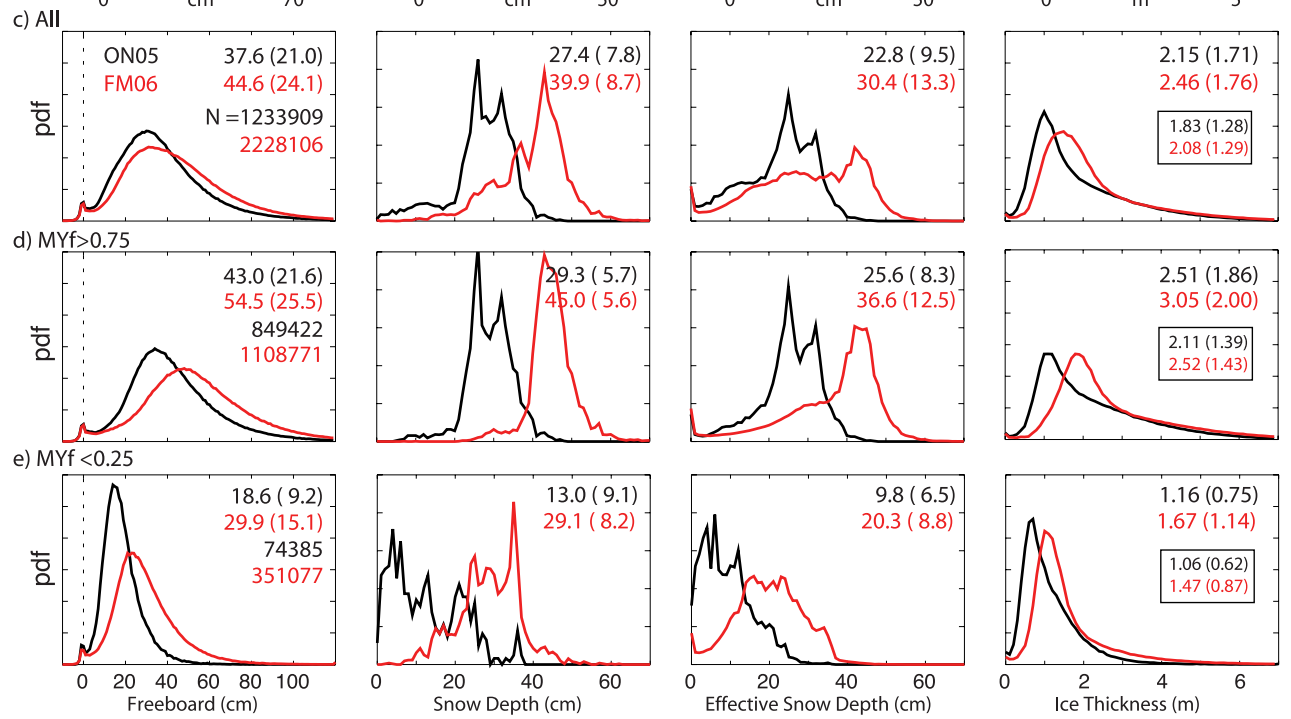
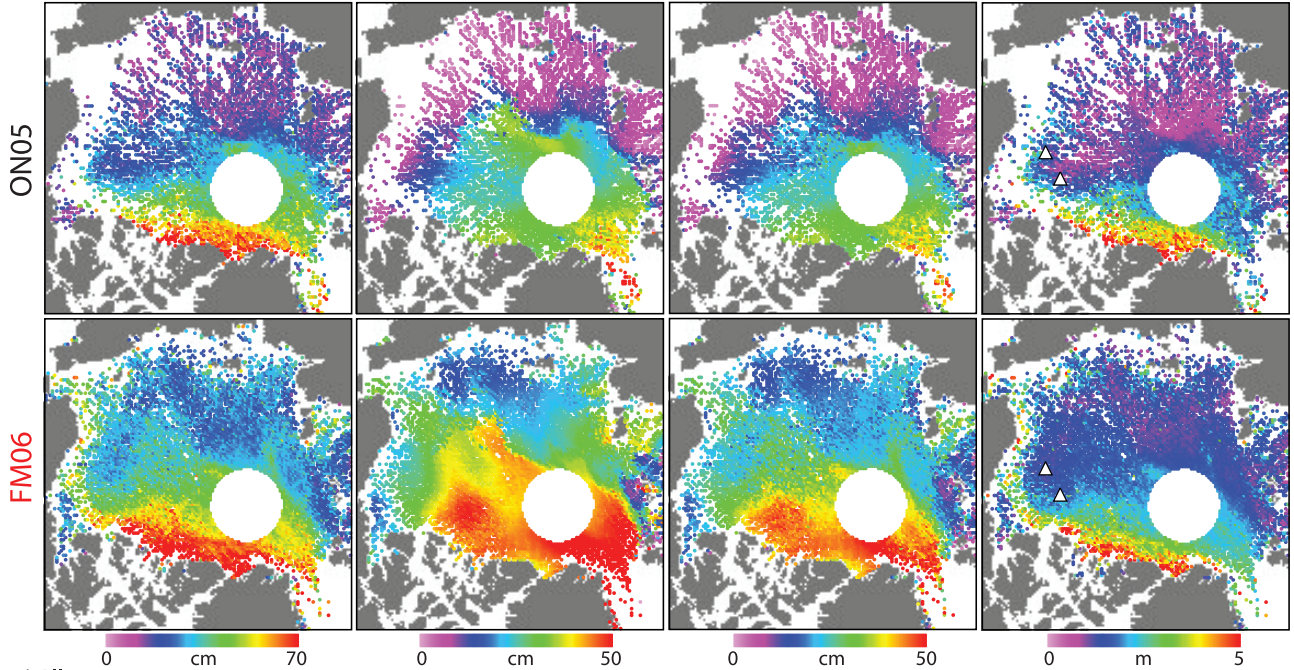
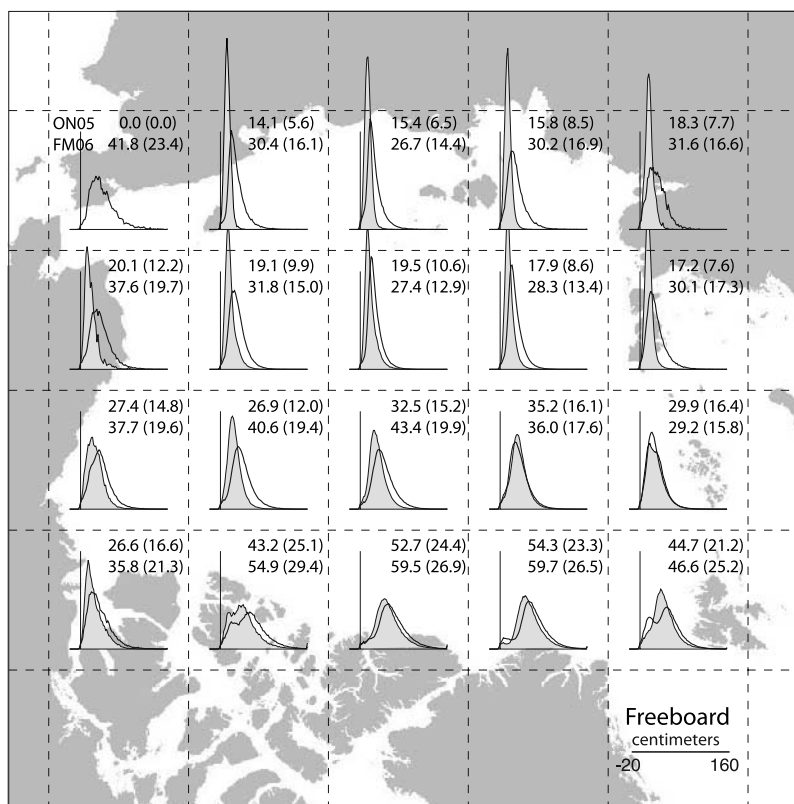


Figure 4



**Figure 5.** Comparison of the freeboard distributions in ON05 (gray) and FM06 (no fill). Distributions are of individual freeboard samples (from 70 m ICESat spots) within 25 km segments in each 700 km by 700 km region. Only segments with at least one sea surface reference are used. The means and standard deviations of the freeboard distributions of the two campaigns are shown in the top right corner of each region.

freeboard (thicker ice) are due to ridges and deformed ice. These differences are expressions of regional changes in freeboard due to snow accumulation, ice growth, and ice advection. The changes in freeboard are generally higher in the seasonal ice zone (an increase of 16.3 cm just north of the East Siberian Shelf) and lower over the MY ice cover in the central Arctic and north of Greenland. The rate of ice growth, as mentioned earlier, is highest in the thinner seasonal ice and probably the largest contributor to the increase in freeboard. Over MY ice, the differences are more moderate and can be compared to the expected changes in the Arctic Ocean mean snow depth of 9 cm between the end of October and end of February [Warren *et al.*, 1999].

#### 4. Construction of Fields of Snow Depth

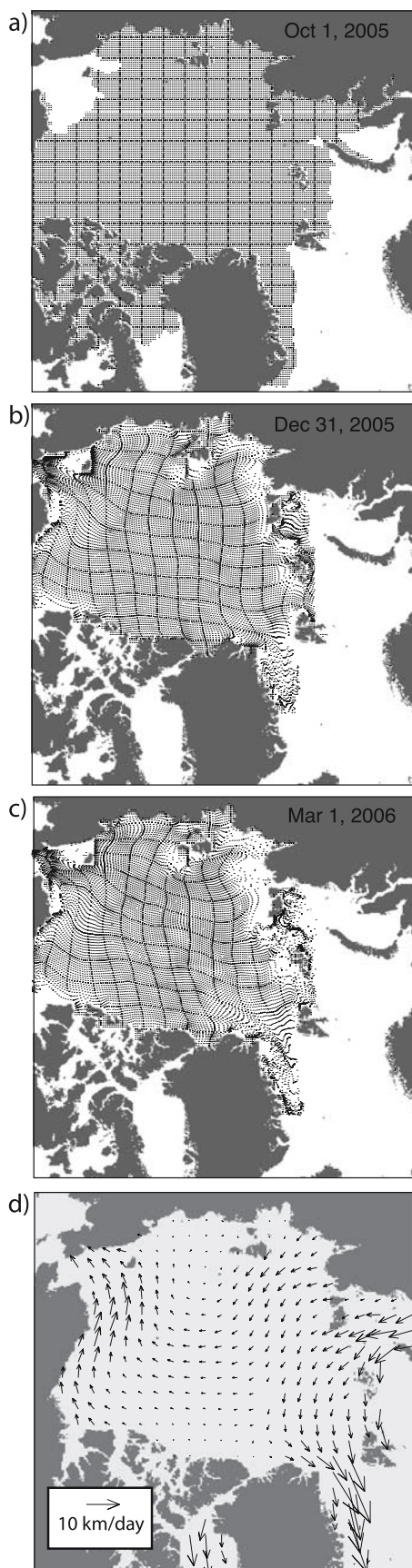
[20] To account for snow loading in the estimation of ice thickness from ICESat, knowledge of both the snow depth and density are required. These parameters are crucial because ICESat freeboard,  $h_f$ , includes the thickness of the snow layer. Since there are no routine measurements of these two spatially and temporally varying quantities over

the Arctic Ocean, our approach is to construct daily fields of snow depth using available climatologies and meteorological products. In this section, we describe the construction of such fields over the fall and winter Arctic sea ice cover and the basis for the selection of certain parameters.

[21] Potentially, one could utilize the snow climatology of the Arctic Ocean sea ice cover by Warren *et al.* [1999]. But this climatology was developed using in situ data collected between 1954 and 1991 and it is not clear how this compilation reflects present-day snow conditions. In addition, it is representative of only snow depth over relatively level multiyear ice and it does not address the snow depth over the increasing expanse of seasonal ice over the Arctic and the changes associated with later onset of freeze and snow accumulation. These same concerns apply to snow density.

[22] Current meteorological fields, however, do provide daily estimates of snow precipitation and thus time- and space-varying estimates of snow conditions. The NCEP/NCAR products include Precipitation-Evaporation (P-E) estimates and the ECMWF products provide actual snowfall, both as Snow Water Equivalent (SWE). Together with some form of climatological snow density, these fields

**Figure 4.** ICESat freeboard, derived snow depth, thickness estimates, and multiyear ice fraction of the ON05 and FM06 campaigns. (a) Multiyear ice fraction from QuikSCAT. (b) Fields of freeboard, snow depth, effective snow depth, and ice thickness. (c) Distributions of freeboard, snow depth, effective snow depth, and ice thickness. (d) The same distributions for areas with multiyear ice fraction  $>0.75$ . (e) The same distributions for areas with multiyear ice fraction  $<0.25$ . N is the number of ICESat freeboard samples in the distributions. The numbers in boxes are results obtained using the thickness-dependent bulk density parameterization of Kovacs [1996].



could be used for construction of daily Arctic snow depth. We have examined the NCEP/NCAR P-E fields but ruled out their use because of the unphysical spatial patterns that are associated with numerical ringing near the poles. Even though it is possible to lessen the effect of these artifacts by spatial filtering, there will still be unwanted residuals and the process further reduces the details in these already coarse spatial estimates.

[23] In view of the above considerations, we elected to use the ECMWF snowfall estimates. To use the ECMWF snowfall estimates effectively, our procedure has to account for: the conditions for accumulation of snow on the ice cover; ice advection; the seasonal variability in snow density; and, the initial snow cover at the end of the summer. Below, we describe the procedures used in the construction of these snowfields and discuss their shortcomings.

#### 4.1. Cycle of Accumulation and Advection

[24] Our snow accumulation process begins on 15 September, before the summer minimum in Arctic Ocean sea ice coverage. Snow accumulation (in SWE) is recorded at daily locations along the drift trajectories of sea ice constructed from AMSR-E 89 GHz motion fields. To accumulate snow correctly, we keep track of the advection of individual ice parcels. Figure 6a shows the initial uniform grid (10-km spacing) before it become deformed with the daily drift of individual particles within the ice cover. The particular example (in Figures 6b and 6c) illustrates the advected field of points on 31 December 2005 and 1 March 2006. Procedurally, a daily cycle of accumulation and ice advection is carried out at each point; this mimics the snow accumulation process in a moving field.

[25] In addition to the above, the following surface conditions determine when and where snow is allowed to accumulate. Accumulation is permitted only when the 2-m air temperature (from the ECMWF fields) is below freezing and the ice concentration (from AMSR-E) is greater than 50%. If the ice concentration were to drop below 50%, the snow is removed from that location. Since ice concentrations rarely drop below 50% inside the perennial pack, these rather simple conditions are more relevant to the accumulation process over seasonal ice during the advance of the ice cover during the fall. With these conditions, there will be less snow where the ice cover is formed later in the season. The initial snow conditions over MY ice are discussed below.

#### 4.2. Snow Density and Depth

[26] Snow density is important because it determines the thickness of the snow layer and thus the fraction of the estimated freeboard that is ice. The variability of snow density is discussed by Warren *et al.* [1999] and Radionov *et al.* [1996]. Warren *et al.* [1999] report that snow density

**Figure 6.** Illustration of the advection of Lagrangian points on the sea ice/snow cover using daily ice motion estimates from the 89-GHz channel of AMSR-E. (a) Initial uniform grid, 10 km spacing. (b) Deformed grid on 31 December 2005. (c) Deformed grid on 1 March 2006. (d) Mean November–March motion field.

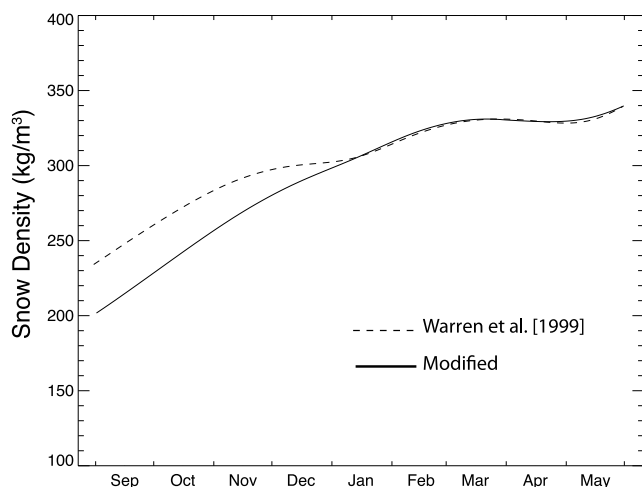


**Figure 7.** Seasonal snow density for conversion of snowfall (in snow water equivalent) to snow depth. The modified version used in this paper is compared to that of *Warren et al.* [1999].

exhibits little geographical variation across the Arctic but that it does vary seasonally: the average snow density for the Arctic Ocean (Figure 7) is only  $\sim 250 \text{ kg/m}^3$  in September but increases with settling and wind packing during the fall and winter to  $320 \text{ kg/m}^3$  in May; the highest density is that of the residual melting snow in July. Even though the winter trend in density is positive, the variability is fairly high; the highest is during the early part of the fall when the density could vary between 100 and  $325 \text{ kg/m}^3$ .

[27] Another feature of the seasonal cycle is that the increases in snow density are highest between September and November but then remains relatively unchanged from December until May. Together with the expected rapid buildup of the snow cover on the sea ice of the Arctic Basin that occurs in September, October and November due to early winter storms (described by *Vowinkel and Orvig* [1970], *Radionov et al.* [1996], *Warren et al.* [1999], and *Sturm et al.* [2002]), there could be significant uncertainty in the estimation of snow depth during these months. Since the snowfall is taken from the ECMWF fields, the question here is: which is the best time-dependent snow density to use in the conversion of SWE to snow depth?

[28] In their paper, *Warren et al.* [1999] show that *Loshchilov* [1964] reports a much lower density ( $\sim 200 \text{ kg/m}^3$ ) in September. In fact, fresh snow has the lowest density ( $50\text{--}90 \text{ kg/m}^3$ ). Since the quantities are measurements of bulk density (i.e., depth integrated), we believe that it is likely that the higher variability in snow density between September and November is due to a large fraction of the fresh snow being accumulated during the early part of the growth season. Hence, this variability of snow density during the late summer and fall significantly affects the conversion of SWE to snow depth and thus our thickness estimation process. On the basis of the above discussion, we use the seasonally varying snow density from *Warren et al.* [1999] but with a modification of shifting the early fall portion of the curve by 1 month which then merges with the original climatology in the late winter (Figure 7). This serves to accommodate the current Arctic climate of longer melt seasons and later freezeups in the Arctic.

#### 4.3. Initial Snow Cover on Multiyear Ice

[29] Another issue that one needs to consider is the initial snow cover (depth and density) over multiyear ice at the beginning of the accumulation season (in our case, 15 September). The initial field represents the snow that survived melt season. Without a realistic thermodynamic and dynamic model of the sea ice cover for simulation of the time-varying ice conditions during the summer, we assume the initial snow cover to be that of the September climatological snow conditions from *Warren et al.* [1999] with a snow density of  $\sim 350 \text{ kg/m}^3$ . In this case, the initial conditions are not time-varying and are identical for the results shown in this work. In our construction, we maintain a separate record of the initial snow conditions (SWE and density) at each grid point.

#### 4.4. Frost Deposition, Sublimation, and Wind Redistribution

[30] In our treatment of the daily snow estimates, we have ignored frost/rime deposition, sublimation, and wind redistribution of snow. We have assumed deposition and sublimation to be negligible: according to an analysis of meteorological data from the NP drifting stations by *Lindsay* [1998, Figure 7], winter sublimation is exceeded by frost deposition. During the 7 months between October and April a net deposition of frost is estimated to contribute  $0.5 \text{ g/cm}^2$ , which is only  $\sim 5\%$  of the total snow accumulation. On the other hand, blowing snow events are important because they are the dominant processes affecting the large-scale surface mass balance of the snow cover over sea ice and thus impact snow depth calculations. Few studies have addressed this topic of wind-driven redistribution; it involves understanding the complex interactions between sea ice surface relief and the atmospheric boundary layer. A recent article by *Déry and Tremblay* [2004] has offered a model for understanding some of the small-scale processes. In any case, advancement in the understanding of this issue requires not only better models, but also better-designed in situ measurements to test the associated simulations.

#### 4.5. Mean Snow Depth for ON05 and FM06

[31] Figure 4 shows the constructed fields of snow depth for the ON05 and FM06 campaigns on a 25-km grid. The value at each grid element represents the mean snow depth (Figure 4b) of all samples within its grid boundaries over that campaign period. The spatial pattern of the basin-scale snow depth maps show clear delineations of the seasonal and multiyear ice zones especially in the fall. This distinct seasonal feature has a close spatial correspondence to the freeboard maps (Figure 4b) and is not reflected in the climatology [*Warren et al.*, 1999]. Broadly, this expected contrast between the two ice zones is a better representation of the behavior of the snow cover: the younger seasonal ice cover formed later in the fall (October and November) has a thinner snow cover than the older ice that survived the summer.

[32] The overall snow depth distribution is shown in Figure 4c. The overall mean snow depth is already 27 cm in ON05 because of the rapid buildup of the snow cover in September, October and November due to early winter storms. The accumulation between the two campaigns is only 13 cm; the mean in FM06 is 40 cm. As in section 3, we separate the FY and MY samples with spatial masks of the

two primary ice types (shown in Figure 4a) to examine only the snow depth distributions between those regions with the predominantly MY ice (>0.75 MY fraction) and those regions with primarily a FY ice cover (i.e., <0.25 MY fraction). The contrast in mean snow depth between the FY and MY ice cover is 16 cm, reflecting the lower accumulation in the seasonal ice cover. Between ON05 and FM06, the increase in the mean snow depth over MY ice is 16 cm, starting with a mean of ~29 cm in the fall. The mean snow depth of the FY ice cover in ON05 is only 13 cm, and has a similar increase in thickness of 16 cm over the ~4 months between campaigns. The relatively low variability in the standard deviation is probably due to the rather coarse resolution of the meteorological fields.

## 5. Estimation of Sea Ice Thickness

[33] This section describes how the retrieved freeboard and the constructed snow cover are combined to estimate sea ice thickness. First, we discuss the parameters required in the equation for computing ice thickness. Second, special considerations on the disparity in the spatial resolution and length scales of some of these parameters are addressed. Third, we provide our estimate of the ice thickness fields from the ON05 and FM06 ICESat campaigns. Last, we examine the sensitivity of the thickness to uncertainties in variables used in the estimation process.

### 5.1. Conversion to Ice Thickness

[34] Assuming that the floating ice cover is in isostatic balance, the relationship between ice thickness ( $h_i$ ), snow depth ( $h_{fs}$ ), and total freeboard ( $h_f$ ) is given by

$$h_i = \left( \frac{\rho_w}{\rho_w - \rho_i} \right) h_f - \left( \frac{\rho_w - \rho_s}{\rho_w - \rho_i} \right) h_{fs}. \quad (4)$$

The densities of ice ( $\rho_i$ ), snow ( $\rho_s$ ), and seawater ( $\rho_w$ ) provide the appropriate scaling for hydrostatic equilibrium. In the following analyses, the density of seawater,  $\rho_w$ , is assumed to be constant (1024 kg/m<sup>3</sup>). The snow bulk density,  $\rho_s$ , follows the seasonal dependence discussed in section 3. We compute sea ice bulk density,  $\rho_i$ , in two ways. In the first approach, we use a constant mean density of 0.925 g/cm<sup>3</sup> [Weeks and Lee, 1958; Schwarz and Weeks, 1977]. The second approach uses the thickness-dependent parameterization of Kovacs [1996],

$$\rho_i = 0.9363 - 0.0018h_{ice}^{0.5} \quad (\text{g/cm}^3). \quad (5)$$

The above equation is derived from measurements of ice cores from the Beaufort Sea and shows that the bulk density decreases with ice thickness. For first-year sea ice, the decrease is associated with brine drainage and growth rate processes, which reduce the volume fraction of the heavier brine entrained within the ice. The lower multiyear ice densities are the result of the inclusion of proportionally less brine and more gas, especially in the freeboard portion, which is nearly low-density fresh ice. In the conversion to ice freeboard, the uncertainty in bulk density is a source of error (as we shall show in section 5.4) even though it varies by only 1.4% between 1 m and 3 m.

### 5.2. Effective Snow Depth

[35] This section addresses how the total freeboard estimates (of individual 70-m ICESat shots) are partitioned into freeboards of ice and snow given mean snow depth estimates from a much larger/coarser length scale. This additional consideration of snow depth resolution is an attempt to make the snowfields compatible with the higher resolution ICESat freeboards. The daily snow depth estimates from section 4 represent the snow accumulation on an ice parcel (10 km by 10 km) once the ice concentration exceeds 50% and the temperature is below freezing. Over multiyear ice, this snow depth is the total accumulation (inclusive of initial snow cover) since 15 September. For seasonal ice, the first date of snow accumulation is variable. In both cases, however, owing to the limits of spatial resolution the snow depth on newly created ice associated with divergence within a resolution element will be overestimated. This is because the large-scale surface conditions (as characterized by the ice concentration/temperature fields) determine the first date of accumulation and do not take into account the actual age of the new openings. That is, the variability of FY ice age within a grid cell is not resolved after the initial creation of that ice parcel, as each new opening starts with zero snow cover.

[36] Thus, rather than taking the sea ice freeboard ( $h_f$ ) to be the difference between just the total freeboard ( $h_f$ ) and the snow depth from above, we have to adjust snow depth to account for the local freeboard variability (associated with new openings as well as the unmodeled redistribution of snow mass) especially when the freeboard is less than the mean snow depth. This ensures that there are no negative sea ice freeboards and that there is a reasonable fraction of ice and snow in the total freeboard. Figure 8 illustrates how the total freeboard is partitioned when the freeboard is close to or less than the large-scale snow depth: the effective snow depth is taken to be a fraction of the total freeboard as defined by the sigmoidal curve. For instance, when the total freeboard is half of the snow depth, one third of the thickness of the total freeboard is partitioned into sea ice and two thirds into snow. Only when the total freeboard is greater than the snow depth (ratio ~1.3) do we get the entire effect of the large-scale snow depth estimate. Our choice of this function is quite arbitrary; the only basis is that there is very little negative freeboard on Arctic sea ice, there is nearly always a snow cover over sea ice, and anecdotal evidence shows that the snow layer could be quite thick even on thin ice.

[37] Differences between the large-scale snow depth and the effective snow depth for ON05 and FM06 can be seen in Figure 4. Overall, the effective snow depth is reduced somewhat (by several centimeters) from the large-scale constructed fields, particularly in regions with larger fractions of seasonal ice. Though this function attempts to address the needs of small-scale variations in snow depth, improvements could certainly be made with better understanding of the distribution of snow at the length scale of the ICESat footprint.

### 5.3. Ice Thickness for ON05 and FM06

[38] Figure 4b shows the maps of ice thickness from the ON05 and FM06 campaigns on a 25-km grid. The value at each grid element represents the mean thickness of 25-km ICESat segments that fall within the grid boundaries. Only 25-km segments that contain sea surface estimates are used in the construction of these thickness maps. The fields from

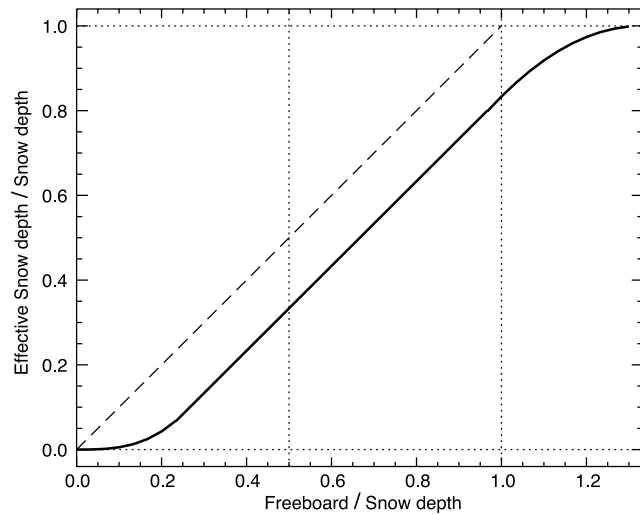


**Figure 8.** Effective snow depth when total freeboard is less than the mean snow depth.

both campaigns retain the expected contrast in thickness between the seasonal and perennial ice zones. The gradient in the spatial fields across the Arctic follow a distinctive pattern with: the thickest multiyear ice next to Ellesmere Island and the Greenland Coast, a gradual thinning toward the central Arctic, and a distinctive transition in thickness from the perennial ice to the seasonal ice cover.

[39] The overall thickness distributions for two campaigns, constructed from available samples, are shown in Figure 4c. Assuming sea ice to have constant density, we obtain a mean thickness of 2.15 m in ON05 and 2.46 m in FM06; an increase of  $\sim 0.3$  m during the 4 months between campaigns. Thickness estimates obtained using the thickness-dependent parameterization of ice density in equation (5) (shown in the insets in Figure 4) are lower because the lower density prescribed for thicker ice gives lower total sea ice mass: the mean thickness becomes 1.83 m in ON05 and 2.08 m in FM06. In addition, we observe fairly long tails in the overall and MY thickness distributions; this is most likely from the thick ice cover adjacent to the northern coast of Greenland, the Lincoln Sea, and the Canadian Archipelago.

[40] As in section 3, we separate the FY and MY samples with spatial masks of the two primary ice types (shown in Figure 4a) to examine only the thickness distributions between those regions with predominantly MY ice ( $>0.75$  MY fraction) and those regions with primarily an FY ice cover (i.e.,  $<0.25$  MY fraction). The increase in the mean thickness of the MY sea ice cover between ON05 and FM06 is 0.5 m [0.4 m], starting with a mean of 2.5 m [2.1 m] in ON05. Values in brackets show the thicknesses derived with the variable bulk density parameterization. In ON05, the mean thickness of the seasonal ice cover is only 1.2 m [1.1 m] with a thickening of 0.5 m [0.4 m] over the  $\sim 4$  months; this is similar to the increase over the MY ice cover. So, at this level of scrutiny, the results seem to be seasonally consistent; that is, there is growth and thickening in both the seasonal and perennial ice zones. Also, this increase in thickness of the MY ice over  $\sim 4$  months, when scaled up to 8 months (i.e.,  $0.5 \text{ m} \times 2$ ) can be compared to the annual cycle (peak-to-trough) of MY ice thickness of  $\sim 1.12$  m from submarine ice draft [Rothrock *et al.*, 2008].

[41] At a more detailed level, we can examine the spatial differences between the two fields. Ideally, only the seasonal differences between ice parcels that share the same initial locations/conditions make sense; otherwise we could be mixing different ice types and ice with different initial conditions and thermodynamic/dynamic histories. Again, ice motion complicates this type of spatial comparison. For our assessment here, we advect the thickness parcels from the ON05 campaign (using AMSR-E ice motion) to their approximate locations in FM06 before computing the differences. The advected ON05 thickness field (Figure 9a) and its differences from the FM06 thickness field in Figure 4 are shown in Figures 9b and 9c. The distribution shows an average thickening of 0.3 m but there are parts of the distribution that show thinning. This is especially evident in the tongue of multiyear ice north of Alaska that continued its westward advection throughout that winter (see Figure 4a): the source region of this ice is the thick ice cover east of the Canadian Archipelago and north of Greenland. We do not think that the negative portion of the distribution is due to melt or noise in the retrieval but due to divergence of the ice cover as that thick ice cover is advected

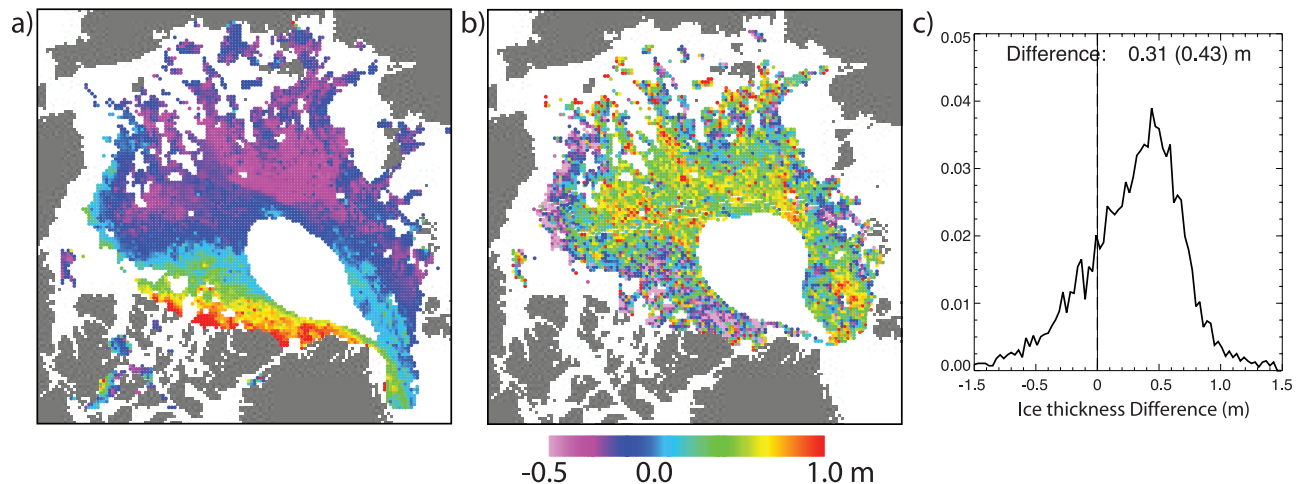


**Figure 9.** Spatial differences in ice thickness. (a) Advected ON05 thickness field. (b) Spatial differences between FM06 and advected thickness field. (c) Distribution of differences.

**Table 1.** Sensitivity of Thickness Estimates  $h_i$  to Uncertainties in the Parameters Used in Equation (4)<sup>a</sup>

$x$	$\sigma_x$	$h_f$	$h_s$	$\frac{\partial h_i}{\partial x}$	$\sigma_x \left( \frac{\partial h_i}{\partial x} \right)$	%var
$h_f$ total freeboard (m)	0.05			9.85	0.49	57-63
$h_s$ snow depth (m)	0.05			6.96	0.35	29-32
$\rho_s$ snow density (kg/m <sup>3</sup> )	100.0	0.43 <sup>b</sup>	0.26 <sup>b</sup>	0.0025	0.25	13
		0.19 <sup>c</sup>	0.10 <sup>c</sup>	0.0010	0.10	2
		0.54 <sup>d</sup>	0.37 <sup>d</sup>	0.0036	0.36	23
		0.30 <sup>e</sup>	0.20 <sup>e</sup>	0.0019	0.19	9
$\rho_i$ ice density (kg/m <sup>3</sup> )	10.0	0.43 <sup>b</sup>	0.26 <sup>b</sup>	0.0233	0.23	11
		0.19 <sup>c</sup>	0.10 <sup>c</sup>	0.0113	0.11	3
		0.54 <sup>d</sup>	0.37 <sup>d</sup>	0.0264	0.26	12
		0.30 <sup>e</sup>	0.20 <sup>e</sup>	0.0150	0.15	5
$\rho_w$ seawater density (kg/m <sup>3</sup> )	1.0	0.43 <sup>b</sup>	0.26 <sup>b</sup>	-0.0217	-0.02	0
		0.19 <sup>c</sup>	0.10 <sup>c</sup>	-0.0104	-0.01	0
		0.54 <sup>d</sup>	0.37 <sup>d</sup>	-0.0247	-0.02	0
		0.30 <sup>e</sup>	0.20 <sup>e</sup>	-0.0140	-0.01	0
$\sigma_{h_i}$					0.69 <sup>b</sup>	
					0.62 <sup>c</sup>	
					0.75 <sup>d</sup>	
					0.65 <sup>e</sup>	

<sup>a</sup>Bulk densities:  $\rho_s = 300$  kg/m<sup>3</sup>,  $\rho_i = 920$  kg/m<sup>3</sup>,  $\rho_w = 1024$  kg/m<sup>3</sup>.

<sup>b</sup>ON05 multiyear ice ( $h_f = 0.43$  m,  $h_s = 0.26$  m from Figure 4).

<sup>c</sup>ON05 first-year ice ( $h_f = 0.19$  m,  $h_s = 0.10$  m).

<sup>d</sup>FM06 multiyear ice ( $h_f = 0.54$  m,  $h_s = 0.37$  m).

<sup>e</sup>FM06 first-year ice ( $h_f = 0.30$  m,  $h_s = 0.20$  m).

south and diverges between the two ICESat campaigns. This divergence, at least at the tongue, can be seen clearly in the MY fields. Since our advection scheme does not account for thickness changes due to divergence, this is not an unreasonable attribution of the results in Figure 9.

#### 5.4. Sensitivity Analysis

[42] At this point, it is useful to examine the uncertainty in the thickness estimates,  $h_i$ , associated with uncertainties in the five variables ( $h_f$ ,  $h_s$ ,  $\rho_w$ ,  $\rho_i$ ,  $\rho_s$ ) in equation (4). Assuming that the variables are uncorrelated, the sensitivity of the thickness estimates can be evaluated according to the following expression:

$$\sigma_{h_i}^2 = \sigma_{h_f}^2 \left( \frac{\partial h_i}{\partial h_f} \right)^2 + \sigma_{h_s}^2 \left( \frac{\partial h_i}{\partial h_s} \right)^2 + \sigma_{\rho_s}^2 \left( \frac{\partial h_i}{\partial \rho_s} \right)^2 + \sigma_{\rho_i}^2 \left( \frac{\partial h_i}{\partial \rho_i} \right)^2 + \sigma_{\rho_w}^2 \left( \frac{\partial h_i}{\partial \rho_w} \right)^2, \quad (6)$$

where

$$\begin{aligned} \frac{\partial h_i}{\partial h_f} &= \frac{\rho_w}{\rho_w - \rho_i}, \\ \frac{\partial h_i}{\partial h_s} &= -\frac{\rho_w - \rho_s}{\rho_w - \rho_i}, \\ \frac{\partial h_i}{\partial \rho_s} &= \frac{h_s}{\rho_w - \rho_i}, \\ \frac{\partial h_i}{\partial \rho_i} &= \frac{\rho_w h_f - (\rho_w - \rho_s) h_s}{(\rho_w - \rho_i)^2} = \frac{h_i}{\rho_w - \rho_i}, \\ \frac{\partial h_i}{\partial \rho_w} &= \frac{-\rho_i h_f + (\rho_i - \rho_s) h_s}{(\rho_w - \rho_i)^2}. \end{aligned}$$

[43] Table 1 shows how uncertainties in the five parameters are propagated into the thickness estimates. The first two partials are functions of the bulk densities of water, ice, and snow while the last three partials are dependent on also the values of total freeboard ( $h_f$ ) and snow depth ( $h_s$ ). In the calculations, we use nominal values of bulk densities:  $\rho_s =$

300 kg/m<sup>3</sup>;  $\rho_i = 920$  kg/m<sup>3</sup>; and  $\rho_w = 1024$  kg/m<sup>3</sup>. To illustrate the seasonal variability of  $\sigma_{h_i}$ , we use the four values of mean freeboard and snow depth of the multiyear and first-year ice covers from the ON05 and FM06 campaigns (Figure 4).

[44] Assigning uncertainties to each variable is more challenging. We do, however, know something about the uncertainties in our tiepoints. There is usually more than one tiepoint within each 25-km segment and they are combined (as described by *Kwok et al.* [2007]) to obtain the best estimate of the sea surface elevation for that segment. The uncertainty of individual tiepoints is dependent on its quality and since the third category of tiepoint dominates the population, we assign  $\sigma_{h_f}$  to be the sample uncertainty of this third category ( $\sim 6$ – $7$  cm; see Figure 3) divided by  $\sqrt{2}$  (i.e., we assume two tiepoints/segment), or  $\sim 5$  cm. We believe this to be a reasonably conservative estimate. As for  $\sigma_{h_s}$ , even though it is not unbounded we simply have to guess; we assign a value of 5 cm. To place this value into context, it represents almost 50%/20% of the snow depth over FY ice and 25%/14% over MY during the ON05/FM05 campaigns. There are many other issues associated with snow depth (discussed in section 4), so this may be an overly optimistic estimate. Better quantification of this value awaits a comprehensive assessment of the ECMWF snowfall fields. Uncertainty in snow density ( $\sigma_{\rho_s}$ ) is taken to be 100 kg/m<sup>3</sup> [see *Warren et al.*, 1999, Figure 11]. Using equation (5) as a guide, we take  $\sigma_{\rho_i}$  to be 10 kg/m<sup>3</sup>; this represents the variability of the bulk density of sea ice between 1 and 3 m. The uncertainty in water density  $\sigma_{\rho_w}$  should be small compared to the other bulk densities and we assume it to be 1 kg/m<sup>3</sup>.

[45] Using the above values, the overall uncertainty in the ice thickness estimates within 25-km ICESat segments is  $\sim 0.7$  m but varies with the relative thickness of the total freeboard and snow depth. Uncertainties are higher over thicker MY ice. It is also clear from Table 1 that the variance of  $h_i$  is explained mostly ( $>80\%$ ) by the uncertainties in total

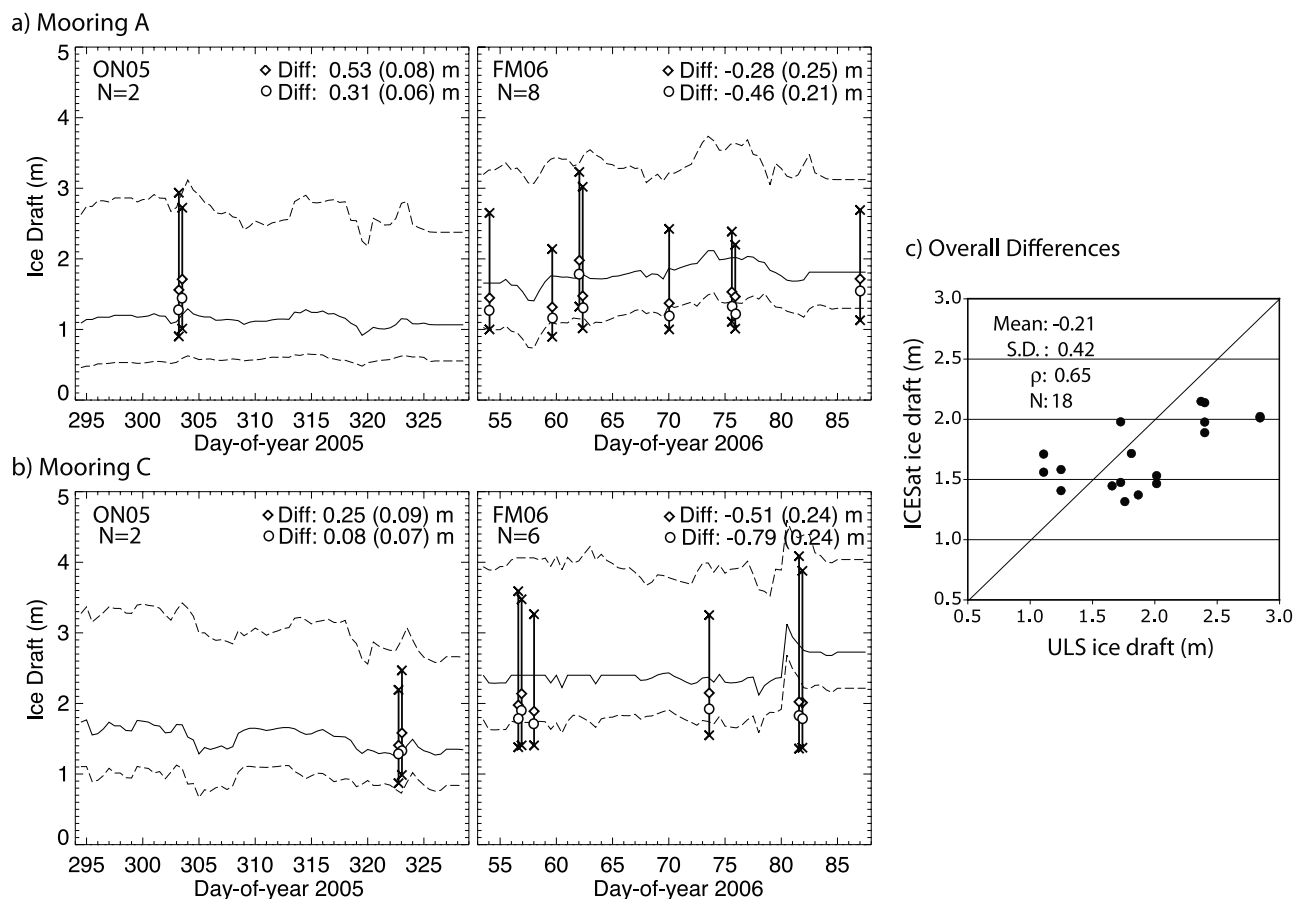


**Figure 10.** Comparison of ice drafts from two WHOI moorings (A and C) with ICESat ice drafts (from 25-km segments) that are within 25 km of the mooring locations. (a) Mooring A. (b) Mooring C. (c) Overall differences. Solid and dashed lines show the time series of the mean and RMS deviations (above and below the mean) of the twice-daily ice draft distributions created from  $\sim 25$  km of ice draft samples centered at the mooring locations. Diamonds and open circles are the ICESat drafts computed using constant and thickness-dependent ice densities. Only the RMS deviations of the constant ice draft distributions are plotted. Ice draft differences/standard deviations from ICESat are shown on the plot. Mooring locations in the Beaufort Sea are shown on Figure 4. (Ice draft data were provided by R. Krishfield, Woods Hole Oceanographic Institution.)

freeboard and snow depth, i.e., the first two terms in equation (6). The contributions of the third and fourth terms are moderate but increase with snow depth and total freeboard: they are typically higher during the winter. Uncertainty in seawater density contributes negligibly to  $\sigma_{h_i}$ . A point to note is that if the thicknesses from individual ICESat segments were truly independent estimates, then averaging them would reduce the uncertainties. More likely, the uncertainties in snow depth estimates are correlated in space because of the resolution of the snowfields and therefore space or time averaging at finer length scales would be less effective.

## 6. Comparison With Ice Draft From Moorings

[46] For an assessment of the ice thickness fields, we turn to ice draft time series from two moorings deployed in the Canada Basin as part of the Beaufort Gyre Observing System ([www.whoi.edu/beaufortgyre](http://www.whoi.edu/beaufortgyre)) [Proshutinsky *et al.*, 2004]. Since 2003, upward-looking sonars (ASL Environmental Sciences model IPS-4) have been located between

50 and 85 m beneath the ice cover (depending on actual mooring length and deployment depth) at the top of three or four bottom-tethered moorings. A directed 420-kHz beam ranges to the bottom surface of the sea ice every 2 s with a footprint of about 2 m. Seawater pressure and temperature are also measured by the instrument every 40 s. Ice draft is determined from the corrected range minus the pressure of the transducer (corrected for atmospheric pressure variations), and taking into account instrument tilt, and sound speed and density variations in the seawater. Raw draft can be in error by as much as 1 m before any corrections are applied. After processing, the estimated error of the ice draft estimates is  $\pm 5$ –10 cm. The locations of the moorings A and C are shown in Figure 4a. During both campaigns, A is located in a zone of mixed first-year and multiyear ice while C is located in a zone of predominantly MY ice; this is evident in the MY fraction analysis in Figure 4.

[47] As the mooring data provide point-wise sampling of the ice draft of a moving ice field at fixed locations and the ICESat profiles provide spatial observations at essentially fixed times, an initial step is to match the spatial length

scales/extent of the observations to produce comparable statistics. Here, the mooring samples are first processed to produce twice-daily samples of the means and standard deviations of ice drafts that are representative of those from 25-km tracks. The total number of mooring observations used in each twice-daily ice draft sample is variable; the temporal interval that brackets the sample population is defined by the time it takes for the overhead ice pack to drift a net distance of  $\sim 25$  km. Ice draft used in this calculation is from the 89-GHz channel of AMSR-E on the Aqua platform. We also note that the ICESat thickness estimates are converted to ice draft for this comparison.

[48] Figure 10 shows the mean and standard deviation of ice drafts from the 25-km ICESat segments that are closest in time and within 25 km of the moorings, and the ice draft time series from the moorings. At mooring A, the differences between the mooring and ICESat ice drafts are: 0.53 m [0.31 m] in ON05, and  $-0.28$  m [ $-0.46$  m] in FM06. For the two campaigns, there are more segments (8 at A and 6 at C) in FM06. The quantities outside and inside the brackets are the mean differences calculated using ICESat draft estimated with constant bulk ice density and with the variable bulk density parameterization (equation (5)), respectively. For reference, the mean (S.D.) of the ice drafts at A are 1.1 (0.1) m in ON05 and 1.8 (0.14) m in FM06. Similarly, at mooring C, the differences are: 0.25 m [0.08 m] in ON05 and  $-0.51$  m [ $-0.79$  m] in FM06. The mean drafts at C are: 1.5 (0.2) m in ON05 and 2.4 (0.2) m in FM06; they are thicker than those at mooring A. As pointed out earlier this thickness contrast is associated with the larger fraction of MY ice at C. The results suggest that, when compared with the moorings, the ICESat-estimated drafts: (1) the ICESat-estimated drafts seem to be slightly overestimated in the fall and underestimated in the winter; and (2) the ICESat-estimated ice drafts calculated using variable ice density behaves as expected; that is, it decreases draft estimates in both fall and winter. Taken together, the overall difference is  $-0.21(0.42)$  m with a correlation of 0.65 between the two ice draft populations (Figure 10c). These values are not inconsistent with our sensitivity analysis presented in the last section. In interpreting the above assessment, it is also important to note that: (1) these comparisons are coincident neither in time nor space and thus variability due to these factors affect the results, and (2) there are inherent uncertainties in the ULS ice drafts ( $\sim 0.1$  m). Typically, the ULS ice drafts are slightly overestimated because the sonar range represents the leading edge of the return pulse from the ice surface and therefore biased by keels if the spot size were large. If this were taken into consideration, it would reduce the differences. Overall, the results are quite encouraging, but they represent only a first assessment over one season. Could the estimates be improved on the basis of the mooring comparisons? Yes, but it would be worthwhile only if there were more years of thickness fields and mooring ice drafts. That is, a more extensive data set in time and space to establish the uncertainties in the estimation process is required.

## 7. Ice Volume/Thickness for Two Winters

[49] In this section, we add to the present discussion the ice thickness estimates from ON06 and MA07. These fields

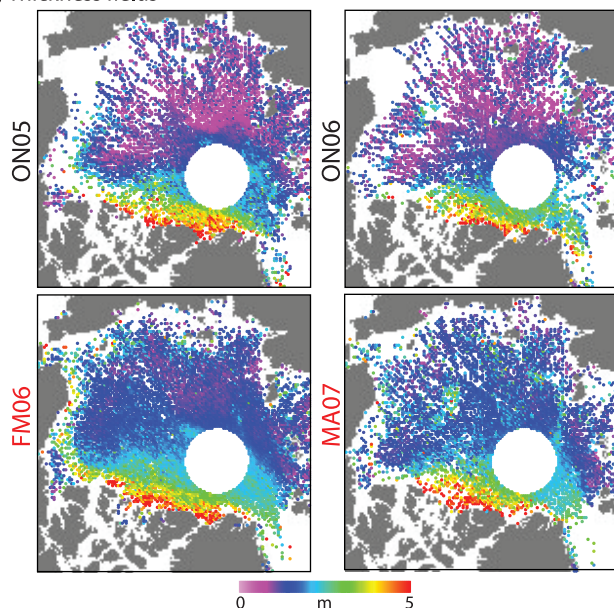
(Figure 11) are derived using the same procedures discussed above. Taking the thickness estimates one step further, we also compute the Arctic Ocean ice volume for the four campaigns (ON05, FM06, ON06, and MA07). These data sets allow a quantitative assessment of the seasonal and interannual changes of ice thickness and ice production, and their consistencies during these two years. At this writing, ice drafts from the Woods Hole moorings for assessment of the ON06 and MA07 thickness fields (as was done in section 6) are not yet available.

[50] The ice thickness fields and their distributions for the four campaigns are shown in Figure 11. For ease of visual comparison, we include the ice thickness distributions of ON05 and FM06 from Figure 4. In terms of thickness, the ON06 mean thickness (1.96 m) is thinner than that in ON05 (2.15 m) by  $\sim 0.2$  m. With a larger expanse of seasonal ice, this is expected. The winter is also thinner, as the overall MA07 mean thickness (2.37 m) is less than that in FM06 (2.46 m) by  $\sim 0.1$  m. The mean thickness of the MA07 field is lower even though the operational period of this campaign started 18 days later (12 March versus 22 February for FM06). The thickness difference of 0.31 m between ON05 to FM06 is less than the increase of 0.41 m between ON06 and MA07. The thicker ice cover may be attributable to the later start date of the MA07 campaign and perhaps the increased ice production associated with relatively larger expanse of seasonal sea ice: basal growth is faster when the ice is thinner. All these broad observations of the seasonal and interannual consistencies of the four fields serve to reinforce our confidence in the results.

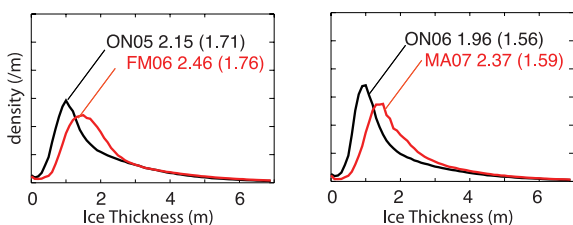
[51] To calculate total Arctic Ocean ice volume, we first fill the gaps in our gridded field of ice thickness, especially the data hole around the North Pole that typically contains a mix of FY and MY ice. For examining the interannual and seasonal variability of ice volume, it is important to have a reasonable estimate of the thickness inside the hole to minimize the effect of advection and the varying coverage of MY and FY ice. In our fill procedure, we assume the MY fraction to be a reasonable proxy of the local average ice thickness. We do this by comparing the values of ice thickness with the corresponding multiyear ice fraction (from QuikSCAT) in the neighborhood of the hole. For each missing grid point, the MY ice fraction at that location is used to provide an estimate of the mean thickness as defined by the correspondence of the neighborhood samples of MY ice fraction and thickness. Even though the hole occupies only  $\sim 7\%$  of the area of the Arctic Ocean, we note that this introduces additional uncertainty in the volume calculations. The filled ice thickness fields are seen in Figure 11. The thickness field is then converted to ice volume simply by multiplying the thickness with the grid cell area and summing over the central Arctic.

[52] From the above procedure, we obtain the following ice volumes within the finite area of the Arctic Ocean bounded by the gateways into the Pacific, the Canadian Archipelago and the Greenland and Barents Seas: 11318, 14075, 10626, and 13891 km<sup>3</sup> for the ON05, FM06, ON06, and MA07 campaigns. Ice production, less ice export, during the  $\sim 4$  months of the ON05-FM06 and ON06-MA07 campaigns is: 2757 and 3265 km<sup>3</sup>. This is equivalent to a growth of 0.37 m and 0.43 m of sea ice covering the  $\sim 7.5 \times 10^6$  km<sup>2</sup> of the Arctic Ocean. These values can be

## a) Thickness fields



## b) Thickness distributions



## c) Interpolated/filled thickness fields

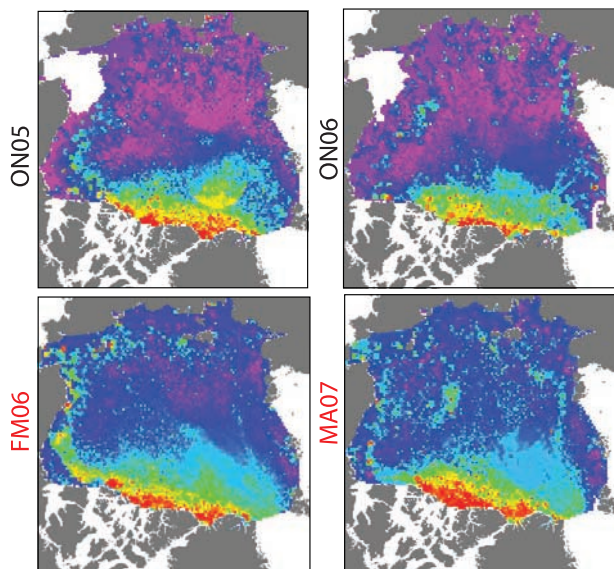


**Figure 11.** Comparison of the four fields from the ON05, FM06, ON06, and MA07 ICESat campaigns. (a) Ice thickness fields. (b) Ice thickness distributions. The mean and standard deviations (units in meters) are shown on the top left corner. (c) Interpolated/filled thickness fields.

compared to the available estimates of annual sea ice growth and melt in the central Arctic Ocean as summarized in Table 1 of *Steele and Flato* [2000]. Briefly, the only mass balance observations from a transect of varying ice thick-

ness give an annual growth of  $\sim 1.1$  m [*Koerner*, 1973]. This annual mean approximately doubles that of the basal growth of  $\sim 0.5$  m over 3 m ice [*Untersteiner*, 1961]. Model estimates of annual production range between 1.1 and 1.3 m. Scaling our 4-month results to an 8-month growth season gives 0.74 m and 0.86 m. Compared to these published values, our estimates of annual ice production are probably underestimated for the following reasons. First, growth rates are not linear, the highest rate of ice production is during late fall and early winter when the seasonal ice cover is relatively thin. By the time of the two October–November ICESat campaigns, the mean thickness of the seasonal ice cover is already over a meter and it covers  $>60\%$  of the Arctic. Realistically, if we had accounted for this ice production, the growth would have been higher. On the other hand, growth slows in the early spring (after March) and perhaps balances out the higher rates during the fall. Second, our ice production estimate is over the entire Arctic Ocean within the physical bounds described earlier, and ice export needs to be accounted for. Taking the mean export to be  $\sim 2200$  km<sup>3</sup> (0.3 m) over the winter [*Kwok et al.*, 2004b], we obtain a figure for annual ice production that is closer to a meter. Given the above considerations, these comparisons of local and basin-scale ice production are necessarily rough. Between the 2 years, the likely reason for the larger ice production during the second year is discussed earlier in this section. In terms of total volume, the larger value in ON05 can be attributed to the higher MY sea ice coverage that year: 37% versus 31% (the MY ice analyses of ON06 and MA07 are not shown here).

## 8. Conclusions

[53] In this examination of ICESat data, we focus on the steps and the considerations in the conversion of retrieved freeboard to estimates of ice thickness, and on an assessment of those estimates. The starting point of this work is the ICESat freeboards from a recent paper [*Kwok et al.*, 2007]. We introduced a nominal adjustment of the elevations of near-sea surface references modified by the presence of an initial snow layer. These adjustments reduced the relative biases between the three categories of tiepoints. Here, we described a procedure for constructing daily fields of snow depth using snowfall from ECMWF meteorological products and offered an approach for partitioning the total freeboard into its snow and ice components. Estimates of ice thickness are then calculated with constant and thickness-dependent bulk densities. Ice draft from ULS moorings in the Beaufort Sea are used to assess these estimates. In this section, we first summarize the results and then highlight some of the assumptions used in obtaining our thickness fields. We hope that this will motivate future studies and observational designs/programs that aim to improve upon the estimation process.

[54] Retrieved freeboards from two ICESat campaigns (ON05 and FM06) are used to illustrate the freeboard/thickness conversion process and to assess the seasonal consistency of the estimates. An additional two thickness fields (ON06 and MA07) are introduced to include an examination of the interannual variability and consistency among the four fields. Assuming constant sea ice bulk density, we obtain mean thicknesses of 2.15/2.46 m in

ON05/FM06 and an overall thinner ice cover of 1.96/2.37 m in ON06/MA07. The results show a growth of  $\sim 0.3$  m and  $\sim 0.4$  m during the  $\sim 4$  months of the ON05-FM06 and ON06-MA07 campaigns. After filling the data hole around the North Pole using a scheme that utilizes QuikSCAT MY analysis, we obtain ice volumes of 11318, 14075, 10626, and 13891 km<sup>3</sup> for the ON05, FM06, ON06, and MA07 periods. The larger ice volume in ON05 versus ON06 can be attributed to the higher MY coverage that fall: 37% versus 31%. But, the estimated ice production is higher in the second year: 3265 versus 2757 km<sup>3</sup>. We attribute this to the later operational period of the MA07 campaign (March/April instead of February/March) and perhaps the larger expanse of seasonal sea ice that led to increased ice production during the fall and winter: basal growth is faster when the ice is thinner. The ice production seems to be within the bounds of values in the published literature (see brief discussion in section 7). Broadly, these fields seem to be seasonally and interannually consistent. The ICESat ice draft from ON05 and FM06 are within 0.5 m of the ice draft measured by moorings at two locations in the Beaufort Sea. Estimates obtained using the thickness-dependent parameterization in equation (5) are slightly lower because the lower density prescribed for thicker ice gives lower total sea ice mass.

[55] In fact, it is quite encouraging that the estimates are within 0.5 m of the ice draft at the two moorings given the general uncertainty and lack of knowledge of some processes. Our analysis of how uncertainties in the variables in equation (4) propagate into the thickness estimates gives a value of  $\sigma_{h_i} \sim 0.7$  m. There are a number of free parameters and assumptions in the construction of the daily snowfields, and the use of these fields for the estimation of thickness. We list some of the knowledge gaps that need to be bridged for improvements of the estimation process: (1) the conditions for the deposition and accumulation of snow on the ice surface; (2) the seasonal cycle of snow density; (3) the method for partitioning the total freeboard into the snow and ice components given the disparity in the resolution of the laser footprint and the resolution of the snowfields; (4) the wind-driven redistribution of snow; (5) the general validity of the thickness-dependent bulk density parameterization; and (6) the validity of the assumption of hydrostatic equilibrium over the ICESat footprint. Certainly, this is by no means an exhaustive list except that these gaps have been encountered and to some extent addressed in our conversion from freeboard to thickness. We should emphasize that, in the design of any observational strategy for acquiring data to tackle some of these issues, one of the most important considerations is the length scale and extent of the data sets: the sample population should be of sufficient size to not only cover the ICESat footprints but also to understand its variability in space and time. Otherwise, it would be difficult to support the design of improved procedures for thickness estimation.

[56] The ice draft time series from the two moored upward-looking sonars have been useful for assessment of the ice thickness estimates. But these are positioned in areas of moderate ice freeboards with moderate snow covers. To better assess the skill of any approach, it is critical to examine extremes in thicknesses and snow conditions, i.e., in areas where the skills of the procedures and the

quality of data are challenged. For example, the areas of thickest ice north of Greenland, the Lincoln Sea, or west of the Canadian Archipelago where there is a residual snow cover from the summer but with relatively average snowfall; in the Fram Strait region, where the storms from the Greenland Sea bring significant precipitation; and, the thinner ice areas in the seasonal ice zone where uncertainties in snow depth introduce large relative errors in the estimated thickness. Even though it is unrealistic to carry out an extensive validation program, a few well-placed moorings would be useful for the routine assessment of the quality of the retrieval process. The utility of these ICESat estimates is dependent on a sustained effort in the evaluation of these fields.

[57] The present examination of ICESat data has focused on the estimation of the ice thickness from four ICESat campaigns. The results show that the ICESat thickness estimates are potentially useful for providing a basin-scale view of the Arctic Ocean, but there are issues that need to be addressed for a better understanding of the quality of these estimates. At this writing, there have been 12 operational periods. Our next steps are directed at continued evaluation of the ICESat freeboard and thickness, the improvement of the retrieval process, and the assessment of the results using available ice draft data from moorings and submarines.

[58] **Acknowledgments.** We wish to thank R. Krishfield at WHOI for providing the ice draft data from the Beaufort Gyre Observing System and D. Perovich at CRREL for providing the results showing the dependence of albedo on snow depth. The ECMWF meteorological products are provided by the Data Support Section of the Scientific Computing Division of the National Center for Atmospheric Research (NCAR). NCAR is supported by grants from the National Science Foundation. The AMSR-E brightness temperature and ice concentration fields are provided by World Data Center A for Glaciology/National Snow and Ice Data Center, University of Colorado, Boulder, Colorado. This work was carried out at the Jet Propulsion Laboratory, California Institute of Technology, under contract with the National Aeronautics and Space Administration.

## References

- Déry, S. J., and L.-B. Tremblay (2004), Modeling the effects of wind redistribution on the snow mass budget of polar sea ice, *J. Phys. Oceanogr.*, *34*, 258–271, doi:10.1175/1520-0485(2004)034<0258:MTEOWR>2.0.CO;2.
- Forsberg, R., and H. Skourup (2005), Arctic Ocean gravity, geoid and sea-ice freeboard heights from ICESat and GRACE, *Geophys. Res. Lett.*, *32*, L21502, doi:10.1029/2005GL023711.
- Holloway, G., and T. Sou (2002), Has Arctic sea ice rapidly thinned?, *J. Clim.*, *15*, 1691–1701, doi:10.1175/1520-0442(2002)015<1691:HASIRT>2.0.CO;2.
- Koerner, R. M. (1973), The mass balance of the sea ice of the Arctic Ocean, *J. Glaciol.*, *12*, 173–185.
- Kovacs, A. (1996), Sea ice: Part II. Estimating the full-scale tensile, flexural, and compressive strength of first-year ice, *Rep. 96-11*, Cold Reg. Res. and Eng. Lab., Hanover, N. H.
- Kwok, R. (2004), Annual cycles of multiyear sea ice coverage of the Arctic Ocean: 1999–2003, *J. Geophys. Res.*, *109*, C11004, doi:10.1029/2003JC002238.
- Kwok, R., A. Schweiger, D. A. Rothrock, S. Pang, and C. Kottmeier (1998), Sea ice motion from satellite passive microwave data assessed with ERS SAR and buoy data, *J. Geophys. Res.*, *103*(C4), 8191–8214.
- Kwok, R., H. J. Zwally, and D. Yi (2004a), ICESat observations of Arctic sea ice: A first look, *Geophys. Res. Lett.*, *31*, L16401, doi:10.1029/2004GL020309.
- Kwok, R., G. F. Cunningham, and S. S. Pang (2004b), Fram Strait sea ice outflow, *J. Geophys. Res.*, *109*, C01009, doi:10.1029/2003JC001785.
- Kwok, R., G. F. Cunningham, H. J. Zwally, and D. Yi (2006), ICESat over Arctic sea ice: Interpretation of altimetric and reflectivity profiles, *J. Geophys. Res.*, *111*, C06006, doi:10.1029/2005JC003175.
- Kwok, R., G. F. Cunningham, H. J. Zwally, and D. Yi (2007), Ice, Cloud, and land Elevation Satellite (ICESat) over Arctic sea ice: Retrieval of freeboard, *J. Geophys. Res.*, *112*, C12013, doi:10.1029/2006JC003978.

- Lindsay, R. W. (1998), Temporal variability of the energy balance of thick arctic pack ice, *J. Clim.*, *11*, 313–333, doi:10.1175/1520-0442(1998)011<0313:TVOTEB>2.0.CO;2.
- Loshchilov, V. S. (1964), Snow cover on the ice of the central Arctic, (in Russian), *Probl. Arct. Antarct.*, *17*, 36–45.
- Proshutinsky, A., R. Krishfield, E. Carmack, F. McLaughlin, S. Zimmerman, K. Shimada, and M. Itoh (2004), Annual freshwater and heat content from 2003–2004: First results from the Beaufort Gyre Observing System, *Eos Trans. AGU*, *85*(47), Fall Meet. Suppl., Abstract C41A-0182.
- Radionov, V. F., N. N. Bryazgin, and Y. I. Aleksandrov (1996), *The Snow Cover of the Arctic Basin* (in Russian), 102 pp., Gidrometeoizdat, St. Petersburg, Russia. (English translation, *Tech. Rep. APLUW TR 9701*, 98 pp., Polar Sci. Cent., Univ. of Wash., Seattle, 1997.)
- Rothrock, D. A., Y. Yu, and G. A. Maykut (1999), Thinning of the arctic sea ice cover, *Geophys. Res. Lett.*, *26*(23), 3469–3472, doi:10.1029/1999GL010863.
- Rothrock, D. A., J. Zhang, and Y. Yu (2003), The arctic ice thickness anomaly of the 1990s: A consistent view from observations and models, *J. Geophys. Res.*, *108*(C3), 3083, doi:10.1029/2001JC001208.
- Rothrock, D., D. B. Percival, and M. Wensnahan (2008), The decline in arctic sea-ice thickness: Separating the spatial, annual, and interannual variability in a quarter century of submarine data, *J. Geophys. Res.*, *113*, C05003, doi:10.1029/2007JC004252.
- Schwarz, J., and W. F. Weeks (1977), Engineering properties of sea ice, *J. Glaciol.*, *19*, 499–530.
- Steele, M., and G. Flato (2000), Sea ice growth, melt, and modeling, in *The Freshwater Budget of the Arctic Ocean*, edited by E. Lyn Lewis, pp. 549–587, Kluwer Acad., Norwell, Mass.
- Sturm, M., J. Holmgren, and D. K. Perovich (2002), Winter snow cover on the sea ice of the Arctic Ocean at the Surface Heat Budget of the Arctic Ocean (SHEBA): Temporal evolution and spatial variability, *J. Geophys. Res.*, *107*(C10), 8047, doi:10.1029/2000JC000400.
- Tucker, W. B., III, J. W. Weatherly, D. T. Epler, D. Farmer, and D. L. Bentley (2001), Evidence for rapid thinning of sea ice in the western Arctic Ocean at the end of the 1980s, *Geophys. Res. Lett.*, *28*(14), 2851–2854, doi:10.1029/2001GL012967.
- Untersteiner, N. (1961), On the mass and heat budget of Arctic sea ice, *Arch. Meteorol. Geophys. Bioklimatol., Ser. A.*, *12*, 151–182.
- Vowinkel, E., and S. Orvig (1970), The climate of the north polar basin, in *World Survey of Climatology*, vol. 14, *Climates of the Polar Regions*, edited by S. Orvig, pp. 129–252, Elsevier, New York.
- Wadhams, P., and N. R. Davis (2000), Further evidence of ice thinning in the Arctic Ocean, *Geophys. Res. Lett.*, *27*(24), 3973–3975, doi:10.1029/2000GL011802.
- Warren, S. G., I. G. Rigor, N. Untersteiner, V. F. Radionov, N. N. Bryazgin, Y. I. Aleksandrov, and R. Colony (1999), Snow depth on Arctic sea ice, *J. Clim.*, *12*, 1814–1829, doi:10.1175/1520-0442(1999)012<1814:SDOASI>2.0.CO;2.
- Weeks, W. F., and O. S. Lee (1958), Observation on the physical properties of sea ice at Hopedale, Labrador, *Arctic*, *11*(3), 134–155.
- Wingham, D. J., et al. (2006), CryoSat: A mission to determine the fluctuations in Earth's land and marine ice fields, *Adv. Space Res.*, *37*(4), 841–871, doi:10.1016/j.asr.2005.07.027.
- Zwally, H. J., et al. (2002), ICESat's laser measurements of polar ice, atmosphere, ocean, and land, *J. Geodyn.*, *34*, 405–445, doi:10.1016/S0264-3707(02)00042-X.
- Zwally, H. J., D. Yi, R. Kwok, and Y. Zhao (2008), ICESat measurements of sea ice freeboard and estimates of sea ice thickness in the Weddell Sea, *J. Geophys. Res.*, *113*, C02S15, doi:10.1029/2007JC004284.

---

G. F. Cunningham and R. Kwok, Jet Propulsion Laboratory, California Institute of Technology, 4800 Oak Grove Drive, Pasadena, CA 91109, USA. (ron.kwok@jpl.nasa.gov)